2572
doi:10.1017/S1431927622009801
Microsc. Microanal. 28 (Suppl 1), 2022

Imaging Nanomagnetism in 3D: Potential Improvements for Vector Electron Tomography Reconstruction

George R. Lewis[1,2*], Emilie Ringe[1,2], Paul Midgley[1]

[1.] Department of Materials Science and Metallurgy, University of Cambridge, Cambridge, UK.
[2.] Department of Earth Sciences, University of Cambridge, Cambridge, UK.
* Corresponding author: grl31@cam.ac.uk

3D nanomagnetism exhibits a range of novel physical properties that stem from a mixture of geometry, topology, and chirality constraints [1]. Methods for its experimental characterisation include: x-ray vector tomography [2]; micromagnetics combined with scalar electron tomography [3]; and vector electron tomography (VET) [4–6]. VET in particular offers both excellent spatial and phase resolution, and these promising studies have established successful experimental protocols. However, the VET reconstruction process is comparatively unexplored, and it is expected that significant improvements in reconstruction quality can be gained through new algorithms (as was the case during the development of scalar electron tomography). In this work we present a novel magnetic VET algorithm and compare it to the current 'conventional' procedure. Our results show that the approach of directly reconstructing magnetic vector potential $\boldsymbol{A}$ instead of the magnetic field $\boldsymbol{B}$, and enforcing wavelet regularisation, can significantly improve the quality of the output for this new imaging mode.

The conventional VET algorithm (which is broadly followed by references [4–6]) uses a dual-axis acquisition scheme, where the x and y tilt series are each used to reconstruct the component of the magnetic field $\boldsymbol{B}$ parallel to their tilt axis (the tilt axis remains perpendicular to the electron beam at all tilts, and consequently remains sensitive to the component of $\boldsymbol{B}$ in that direction). A standard SIRT (simultaneous iterative reconstruction technique) routine is used for reconstructing B_x and B_y; then B_z is derived from these using Maxwell's zero divergence law (Figure 1a). However, one major issue with this approach is that since each projection contains a mixture of contributions from B_x, B_y and B_z, using each projection to reconstruct only one component means the collected data is not being used to its full capacity. This leads to several reconstruction artefacts, most noticeably a low quality B_z due to error propagation.

Our new VET algorithm relies on the fact that the magnetic phase change is proportional to the magnetic vector potential $\boldsymbol{A}$ projected along the electron beam direction. This allows us to decompose the initial phase images into individual components of $\boldsymbol{A}$ using a series of geometric weightings w, and use these to reconstruct the potential directly using three separate reconstructions. We employ wavelet regularisation [7] during the reconstruction since it allows us to incorporate the prior knowledge that $\boldsymbol{A}$ can be sparsely represented by certain wavelet transforms. This process is iterated, using adaptive thresholds to adjust which images should contribute towards each component. This results in a high-quality reconstruction of $\boldsymbol{A}$ that can then be simply converted into $\boldsymbol{B}$ (Figure 1b).

We tested the new and conventional algorithms using a simulated holography dataset of a hopfion core; a novel 3D topological soliton with promising magnetic properties which resembles a skyrmion twisted into a ring (chosen for its challenging 3D magnetisation structure). The hopfion magnetisation was calculated following the analytical approach in [8], and used to calculate projected phase images ϕ (tilt range of ±70°, 10 images each for x and y tilt axes) [9]. These 'ideal' phase images were subsequently

modified by simulating their corresponding electron hologram with experimental noise and extracting the final 'realistic' phase images used for reconstructions (Figure 2a). We measured algorithm performance using two complementary metrics: coefficient of determination (R^2, averaged over B_x, B_y, and B_z) was used to probe the similarity in magnitude between phantom and reconstructed $\boldsymbol{B}$ fields; and mean cosine similarity (calculated using θ, the angle between phantom and reconstructed $\boldsymbol{B}$ vectors) was used to probe the similarity in directions of the magnetic field.

We found that the new algorithm significantly out-performs the conventional approach across both magnitude and direction metrics (Figure 2b), and visually results in a much better match to the phantom, particularly when examining the z component of the field (Figure 2c). Furthermore, our algorithm is more robust to noise and comparatively more stable with respect to the choice of the number of iterations; the comparatively broad plateau makes it less likely to choose a value that will be corrupted by noise fluctuations (Figure 2b). Additionally, our algorithm is not necessarily restricted to dual-axis collection schemes, which is a significant advantage as it allows for flexibility when experimental conditions limit the field of view during imaging.

In conclusion, we have developed a new reconstruction algorithm for magnetic VET that significantly outperforms the existing conventional algorithm, further improving the utility of magnetic VET as a novel imaging mode. This was achieved using a process that iteratively unmixes components of the magnetic vector potential with a regularised reconstruction approach. In future work we hope to benchmark the new algorithm over a greater variety of test scenarios, including experimental data [9].

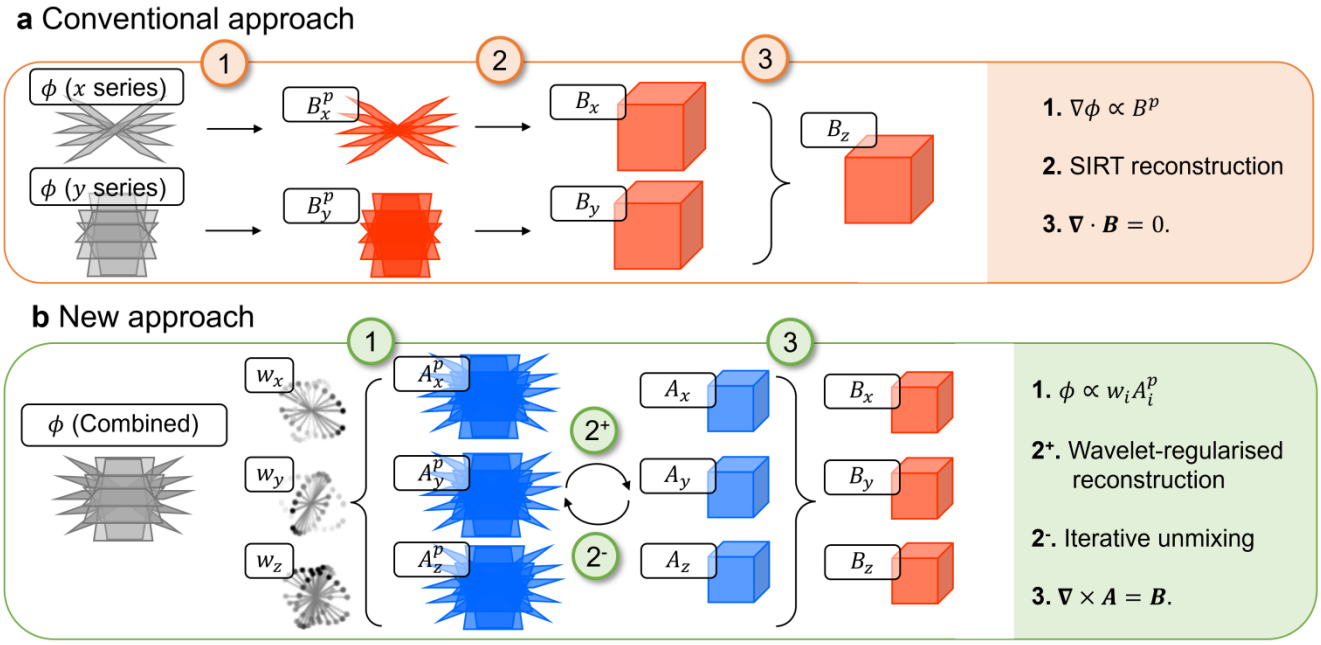

Figure 1. Magnetic electron tomography reconstruction schemes. (a) The conventional scheme processes phase images ϕ from each tilt series separately as projections of the magnetic field B^p. (b) Our new scheme uses geometric weightings w to convert the phase images into projections of the magnetic vector potential A^p before converting directly to B at the end.

https://doi.org/10.1017/S1431927622009801 Published online by Cambridge University Press

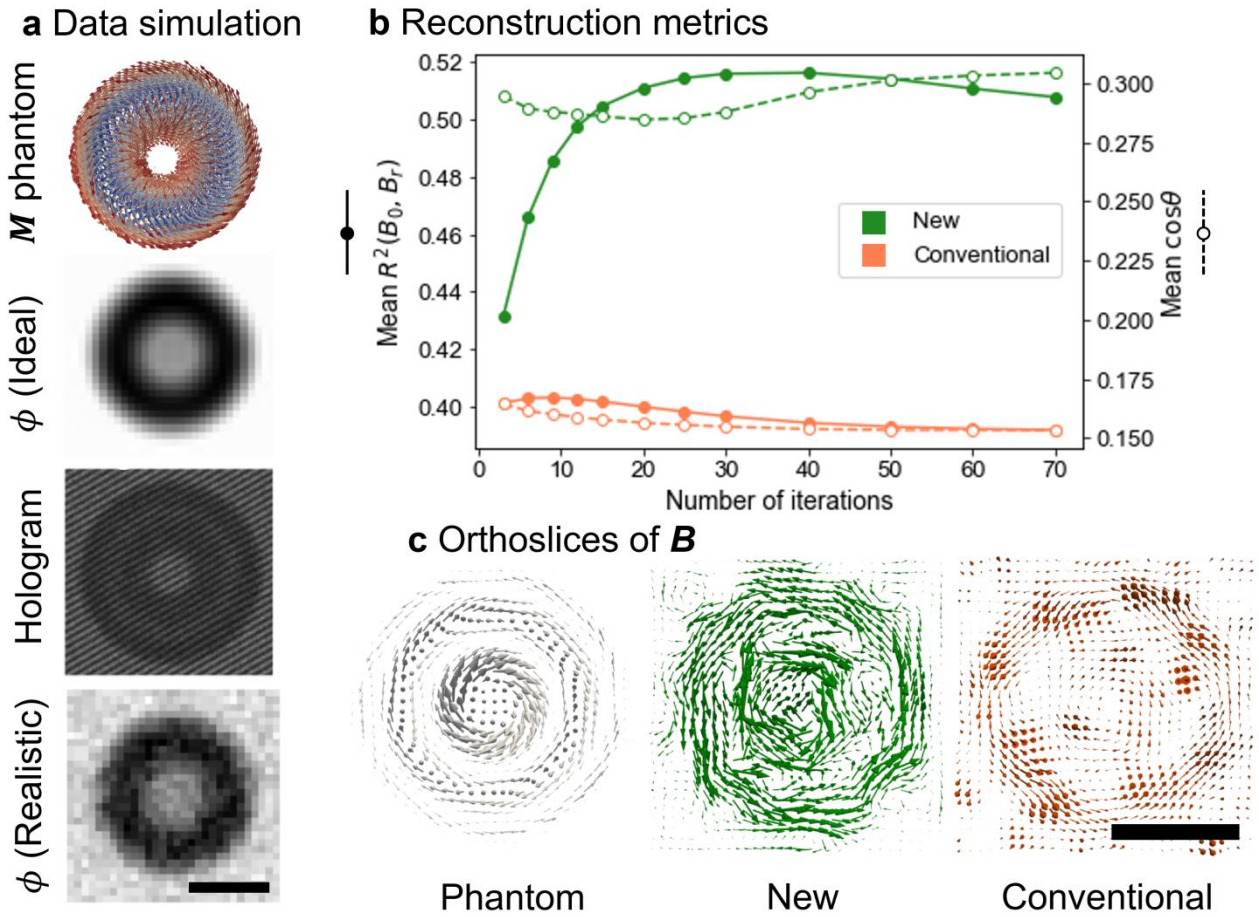

Figure 2. Reconstruction performance for a simulated hopfion core. (a) Process of simulating a magnetic tomography dataset, illustrated for a single projection direction. (b) Performance of new and conventional algorithms as a function of the number of tomographic iterations, showing both a measure of magnitude similarity (mean R^2 value, left) and direction similarity (mean cosθ, right) when comparing the phantom B_0 and reconstructed B_r magnetic fields. (c) Central z orthoslices of the hopfion phantom and its reconstruction by new and conventional algorithms. Scalebars in (a) and (c) are 100 nm.

References:

[1] A. Fernández-Pacheco et al., *Nat. Commun.* **8** (2017) 15756. doi:10.1038/ncomms15756.
[2] C. Donnelly et al., *Nature*. **547** (2017) 328–331. doi:10.1038/nature23006.
[3] G.R. Lewis et al., *Nano Lett.* **20** (2020) 7405–7412. doi:10.1021/acs.nanolett.0c02795.
[4] D. Wolf et al., *Nat. Nanotechnol. 2021*. (2021) 1–6. doi:10.1038/s41565-021-01031-x.
[5] T. Tanigaki et al., *Nano Lett.* **15** (2015) 1309–1314. doi:10.1021/nl504473a.
[6] C. Phatak, A.K. Petford-Long, and M. De Graef, *Phys. Rev. Lett.* **104** (2010) 253901. doi:10.1103/PhysRevLett.104.253901.
[7] R. Tovey, (n.d.). https://github.com/robtovey/ToveyTomoTools (accessed February 3, 2022).
[8] P. Sutcliffe, *J. Phys. A Math. Theor.* **51** (2018) 375401. doi:10.1088/1751-8121/AAD521.
[9] M. Beleggia, and G. Pozzi, *J. Electron Microsc. (Tokyo).* **62** (2013). doi:10.1093/jmicro/dft008.
[9] We acknowledge support from the EPSRC NanoDTC Cambridge (EP/L015978/1) and EPSRC grants EP/V007750/1, EP/R008779/1 and EP/N032128/1.